

Electronic Supplementary Information for:

Modular Structure of a Microporous MOF based on Cu₂ Paddle-Wheels with High CO₂ Selectivity

José M. Seco,^a David Fairen-Jimenez,^{b,*} Antonio J. Calahorro,^c Laura Méndez-Liñán,^c Manuel Pérez-Mendoza,^c Nicola Casati,^d Enrique Colacio^c and Antonio Rodríguez-Diéz^{c,*}

^aDepartamento de Química Aplicada, Facultad de Ciencias Químicas de San Sebastián, Universidad del País Vasco, Paseo Manuel Lardizábal 3, 20008 San Sebastián, Spain.

^bDept. of Chemical Engineering & Biotechnology, University of Cambridge, Pembroke Street, Cambridge CB2 3RA, United Kingdom. <http://people.ds.cam.ac.uk/df334>

^cDepartamento de Química Inorgánica, Universidad de Granada, Av. Fuentenueva s/n, 18071, Granada, Spain.

^dPaul Scherrer Institute, WLGA/229, Villigen PSI, 5232, Switzerland.

Email: David Fairen-Jimenez, df334@cam.ac.uk, Antonio Rodríguez-Diéz: antonio5@ugr.es

Index

S1. Experimental Section.....	S1
S2. Type I vs. Type III Deliverable Capacity.....	S5
S3. Structural Information and Pore Size Distribution.....	S6
S4. Gas Adsorption Isotherms.....	S7
S5. High-Pressure X-Ray Diffraction Analysis	S8
S6. References.....	S9

S1. Experimental Section

Synthesis of [Cu₂(glu)₂(μ-bpp)]·2H₂O (1).

The reaction in water solvent of the copper sulfate (0.25mmol, 0.0628 g), glutaric acid (0.25 mmol, 0.033 g), urea (0.872 mmol, 0.054 g) and 4,4'-trimethylene-dipyridine (0.25 mmol, 0.046 g) led to a blue solution, which kept at room temperature for one week gave rise to green crystals of complex 1, which were filtered off and air-dried. Yield: 60%. Anal. Calc. for C₂₃H₂₆Cu₂N₂O₈: C, 47.18; H, 4.48; N, 4.78. Experimental: C, 47.05; H, 4.61; N, 4.83.

Physical Measurements

Microanalysis of C, H and N were performed in a Fisons Instruments EA-1008 analyser. The thermal behaviour of **1** was studied under an air flow in Shimadzu TGA-50 and Shimadzu DSC- 50 equipment, at heating rates of $20\text{ }^{\circ}\text{C min}^{-1}$ and $10\text{ }^{\circ}\text{C min}^{-1}$, respectively. IR spectra were recorded on a ThermoNicolet IR 200 spectrometer using KBr pellets. All this equipment is sited at the Centre of Scientific Instrumentation of the University of Granada.

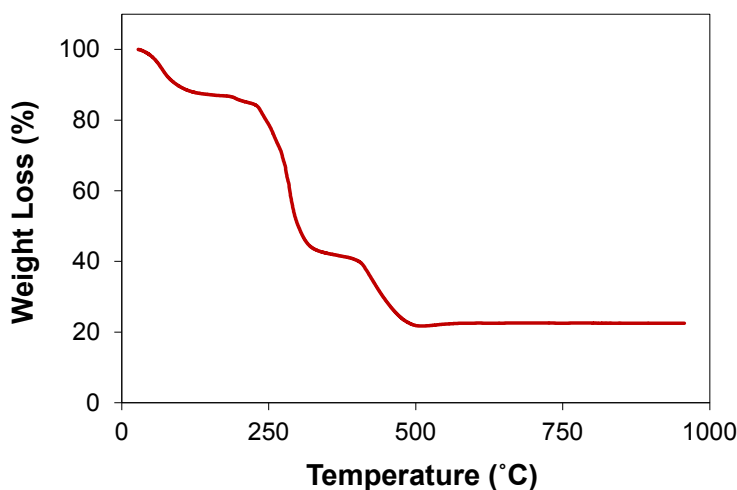


Figure S1. Thermogravimetric curve obtained for **1**.

Single-Crystal Structure Determination.

Suitable crystals of **1** were mounted on a glass fibre and used for data collection on a Bruker AXS APEX CCD area detector equipped with graphite monochromated Mo K α radiation ($\lambda = 0.71073\text{ \AA}$) by applying the ω -scan method. Lorentz-polarization and empirical absorption corrections were applied. The structure was solved by direct methods and refined with full-matrix least-squares calculations on F^2 using the program SHELXS97.¹ Anisotropic temperature factors were assigned to all atoms except for hydrogen atoms, which are riding their parent atoms with an isotropic temperature factor arbitrarily chosen as 1.2 times that of the respective parent. Attempts to identify the solvent molecules failed in compound **1**. Instead, a new set of F^2 (hkl) values with the contribution from solvent molecules withdrawn was obtained by the SQUEEZE procedure implemented in PLATON-94.² Several crystals of **1** were measured and the structure was solved from the best data we were able to collect. Final R(F), wR(F^2) and goodness of fit agreement factors, details on the data collection and analysis can be found in crystal data. Selected bond lengths and angles are given in Tables S1. CCDC reference number for the structure of **1** was xxxxxx.

Table S1. Selected Distances (Å) and Bond Angles (°) for compound 1

N1A C2A 1.331(7)	C2AN1A C6A 116.4(4)	O8B C7B C6B 118.1(4)
N1A C6A 1.340(6)	C2AN1A Cu1 120.8(3)	C3B O1B Cu1 124.9(3)
N1A Cu1 2.161(4)	C6AN1A Cu1 121.8(3)	C3B O2B Cu1 123.3(3)
C2AC3A 1.374(8)	N1A C2A C3A 123.8(5)	C7B O8B Cu1 120.8(3)
C3AC4A 1.383(8)	C2AC3A C4A 120.3(5)	C7B O9B Cu1 126.0(3)
C4AC5A 1.395(7)	C3AC4A C5A 116.2(5)	O8B Cu1 O1B 91.09(17)
C4AC7A 1.512(7)	C3AC4A C7A 124.7(5)	O8B Cu1 O2B 87.62(16)
C5AC6A 1.382(7)	C5AC4A C7A 119.0(5)	O1B Cu1 O2B 168.17(14)
C7AC8A 1.519(6)	C6AC5A C4A 119.8(5)	O8B Cu1 O9B 167.41(14)
C8AC7A 1.519(6)	N1A C6A C5A 123.3(5)	O1B Cu1 O9B 89.27(16)
C3B O1B 1.257(6)	C4AC7A C8A 115.7(5)	O2B Cu1 O9B 89.46(15)
C3B O2B 1.269(6)	C7AC8A C7A 109.9(6)	O8B Cu1 N1A 102.41(15)
C3B C4B 1.482(7)	O1B C3B O2B 123.6(4)	O1B Cu1 N1A 96.39(14)
C4B C5B 1.515(7)	O1B C3B C4B 119.6(4)	O2B Cu1 N1A 95.38(14)
C5B C6B 1.534(6)	O2B C3B C4B 116.8(5)	O9B Cu1 N1A 90.05(15)
C6B C7B 1.506(6)	C3B C4B C5B 116.3(4)	O8B Cu1 Cu1 86.27(11)
C7B O9B 1.240(6)	C4B C5B C6B 111.9(4)	O1B Cu1 Cu1 83.64(10)
C7B O8B 1.246(6)	C7B C6B C5B 112.9(4)	O2B Cu1 Cu1 84.54(10)
C7B C6B 1.506(6)	O9B C7B O8B 125.0(5)	O9B Cu1 Cu1 81.26(11)
O1B Cu1 1.976(3)	O9B C7B C6B 117.0(4)	N1A Cu1 Cu1 171.31(11)
O2B C3B 1.269(6)		
O2B Cu1 1.981(3)		
O8B Cu1 1.970(4)		
O9B C7B 1.240(6)		
O9B Cu1 1.985(4)		
Cu1 Cu1 2.6332(12)		

Gas Adsorption Isotherms

Volumetric N₂ gas adsorption isotherms were undertaken using a Micromeritics Instrument Corporation (Norcross, Georgia, USA) ASAP 2020 system. Approximately 300-500 mg of the corresponding solid product was transferred to a preweighed sample tube and evacuated under dynamic vacuum at 150 °C on the gas adsorption apparatus until the outgas rate was <5 μmHg. The sample tube was reweighed to obtain a consistent mass for the degassed modified product. High-pressure adsorption isotherms of H₂ at 77 K and CH₄ and CO₂ at 273 K were determined using a bench-scale volumetric adsorption instrument equipped with two Baratron absolute pressure transducers (MKS type 627B). Their pressure range span from 0 to 1.33 bar and from 0 to 33.33 bar, respectively. The reading accuracy was 0.05% of the usable measurement range. Prior to all the measurements, samples were degassed at 425 K for 12 h. All gases used were of 99.999% purity. Helium was used for the dead volume determination.

Gas Adsorption Simulations and Computational Structural Characterization

The adsorption of CO₂ was investigated using grand canonical Monte Carlo (GCMC) simulations, performed with the in-house multi-purpose code RASPA.³ We used a rigid atomistic model for **1**, in which the framework atoms were kept fixed at their crystallographic positions. Solid-fluid and fluid-fluid interactions were calculated using a Lennard-Jones (LJ) + Coulomb potential. LJ parameters for the framework atoms were taken from the Universal Force Field (UFF),⁴ the CO₂, LJ parameters from the Trappe force field.⁵ Lorentz-Berthelot mixing rules were used for all cross terms, and LJ interactions beyond 12 Å were neglected. Coulombic interactions were modelled by placing partial charges on the framework atoms. The partial charges were calculated using an extended charge equilibration method,⁶ and the long-range electrostatic interactions were calculated using the Ewald summation method. 6·10⁴ Monte Carlo equilibration cycles were performed plus 4·10⁴ production cycles to calculate the ensemble averages. In one cycle, an average of N moves were performed, where N is the number of molecules in the system (which fluctuates in GCMC). Monte Carlo moves used with equal probability were translation, rotation, insertion, deletion, and random reinsertion of an existing molecule at a new position. To calculate the gas-phase fugacity, we used the Peng-Robinson (PR) equation of state (EOS)⁷.

Table S2. Lennard-Jones parameters for framework atoms and the gas molecules.

	σ [Å]	ϵ/k [K]	q [e]
C	3.431	52.838	
N	3.261	34.722	
O	3.119	30.192	
H	2.571	22.142	
Cu	3.114	62.397	
C_CO ₂	2.800	27.000	+0.70
O_CO ₂	3.050	79.000	-0.35

The pore volume, used to compute excess adsorption from the simulated absolute adsorption, was obtained using a Widom particle insertion method, by probing the structure with a helium molecule at room temperature, recording a large number of random points not overlapping the van der Waals volume of the framework.⁸ The pore size distributions was calculated using the method of Gelb and Gubbins,⁹ where the largest sphere that can fit in a random point within a structure without overlapping the van der Waals surface of the framework is recorded for a large number of random points.

S2. Type I vs. Type III Deliverable Capacity

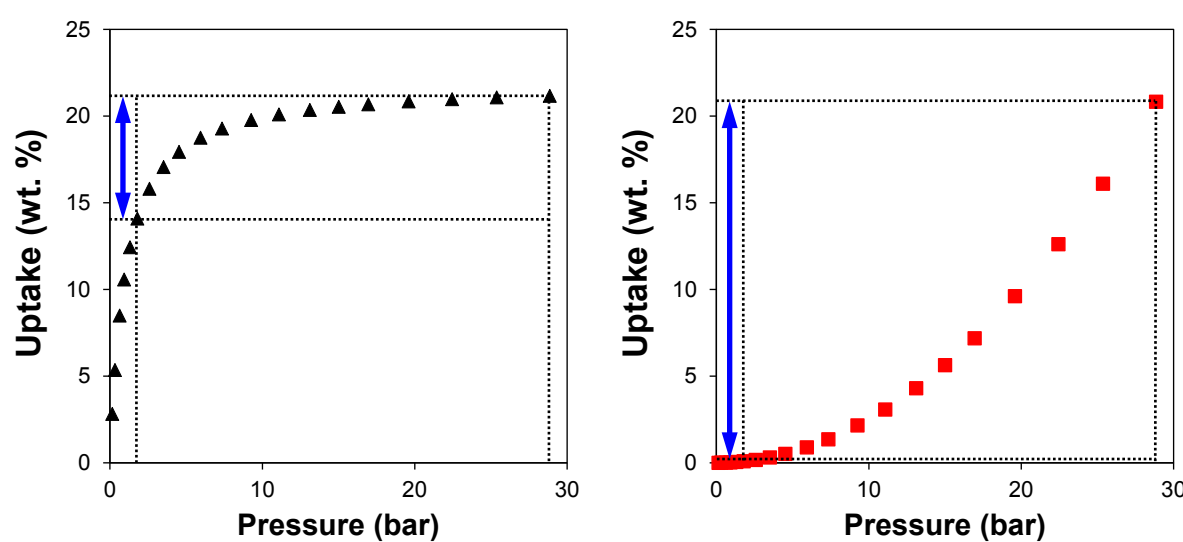


Figure S2. Representation of Type I (*left*) and Type III (*right*) ideal adsorption isotherms. Blue arrows represent the deliverable capacity, *i.e.* the difference between the amount adsorbed at the maximum adsorption pressure and the amount adsorbed at the regeneration pressure,

S3. Structural Information and Pore Size Distribution

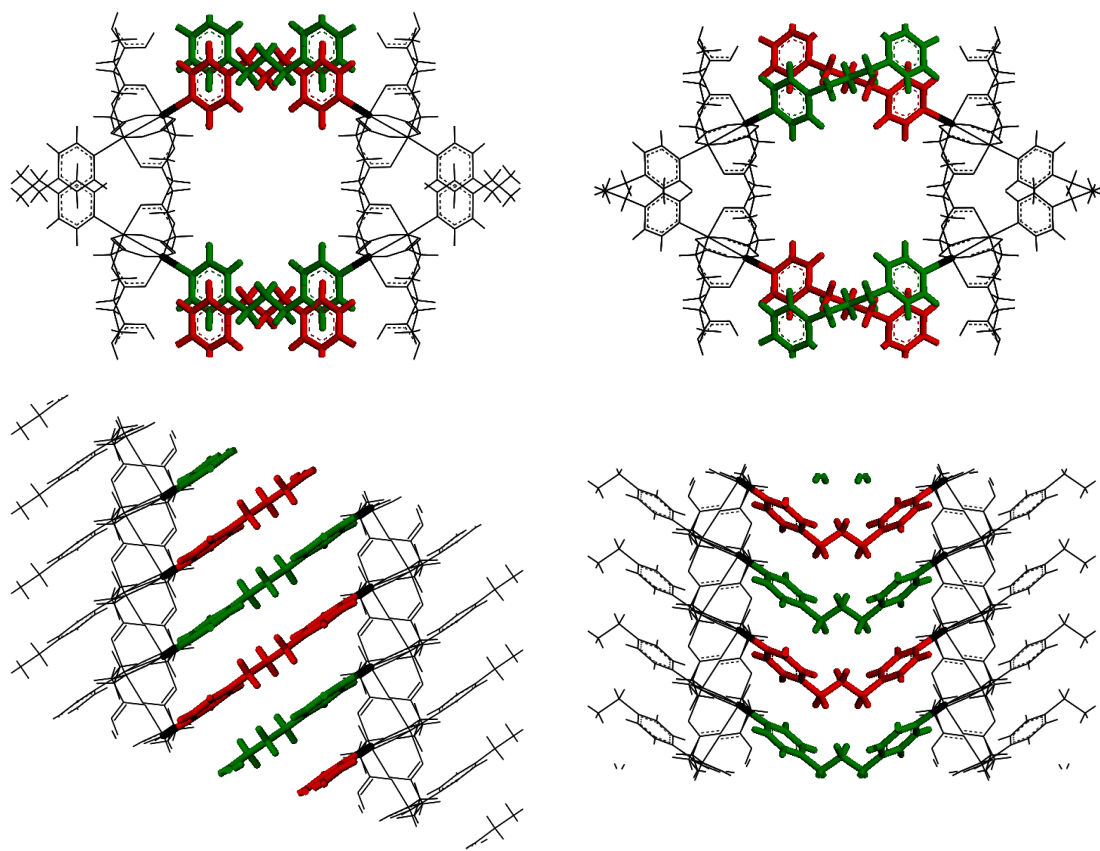


Figure S3. Comparison between the MOF structures (*left*) **1** and (*right*) **2**¹⁰, along the (*top*) *c* and (*bottom*) *b* axis. The different molecular fragments have been indicated in red and green for clarity. Note the different arrangement of the bpp ligands based in the tilt of the pyridyl fragments respect to the propane chain that interconnects them.

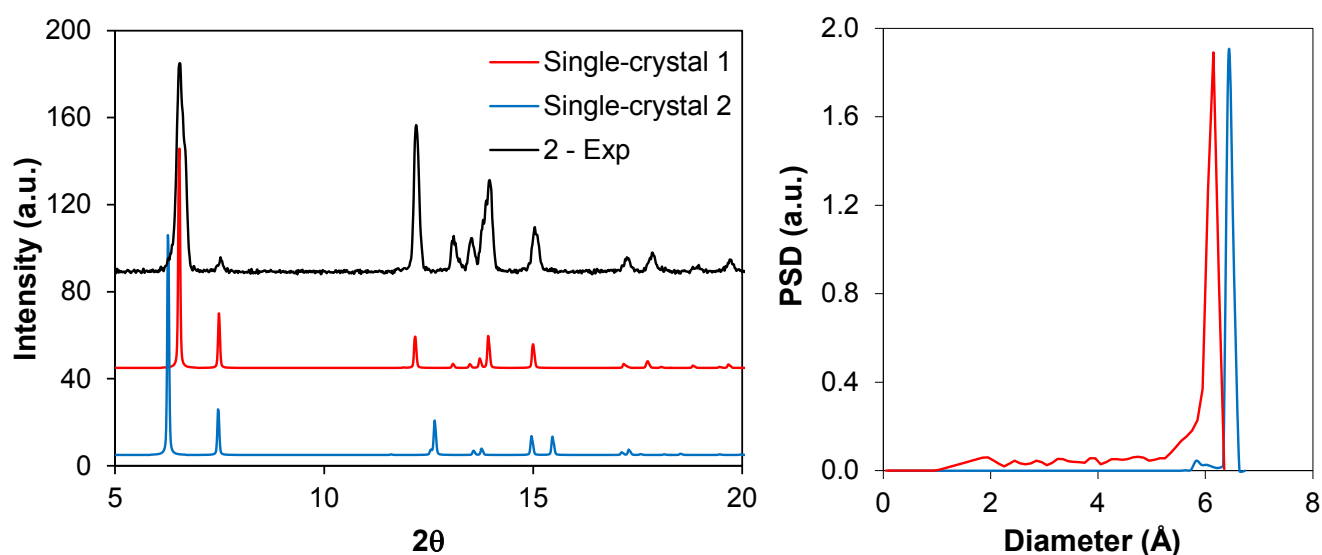


Figure S4. Comparison of experimental XRD pattern (black line) with single-crystal structures (*left*), and pore size distribution (PSD) (*right*). Red line represents single-crystal **1**, and blue line single-crystal **2**.

S4. Gas Adsorption Isotherms

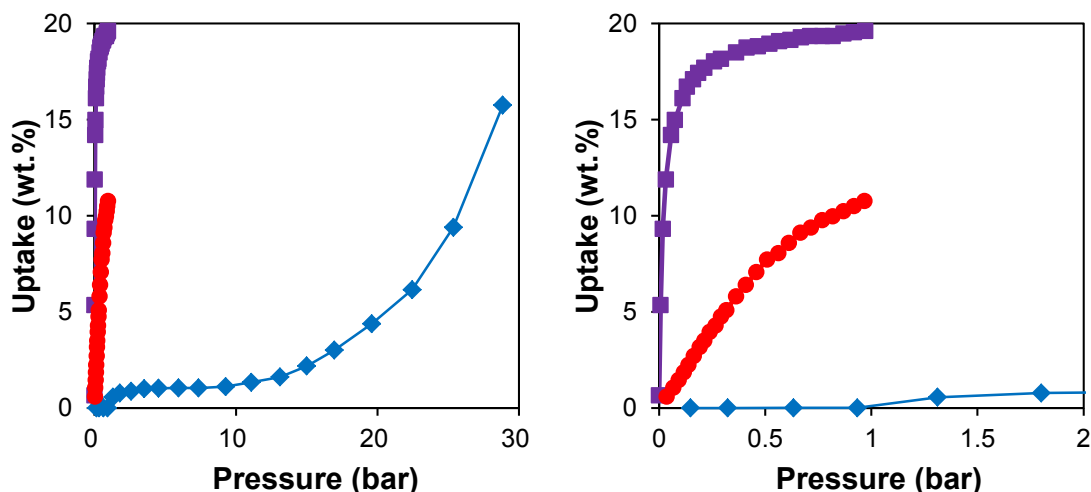


Figure S5. Comparison between the experimental CO₂ adsorption isotherms on structures **1** and **2** at two different temperatures. Blue diamonds, structure **1** at 273 K; red triangles, structure **2** at 273 K; purple squares, structure **2** at 196 K. (*Left*) and (*right*) shows different pressure ranges.

Differences between **1** and **2** are related to the shape of the isotherms:

- i) The CO₂ adsorption capacity of structure **1** up to 2 bar and 273 K is 0.01 wt%. A small plateau exists between 2-10 bar, with an uptake of *ca.* 1 wt %. Both amounts are almost negligible compared with the 15 wt. % uptake obtained at 30 bar.
- ii) Structure **2** adsorbs *ca.* 11 wt. % at 1 bar and 273 K. In addition, the adsorption at lower temperature (196 K) and 1 bar (*i.e.* P/P₀ ~ 0.5, where the whole microporosity should be saturated) increments the uptake up to 19.6 wt.%). The isotherms on **2** keep a Type I shape in all the temperature range (196 – 298 K).

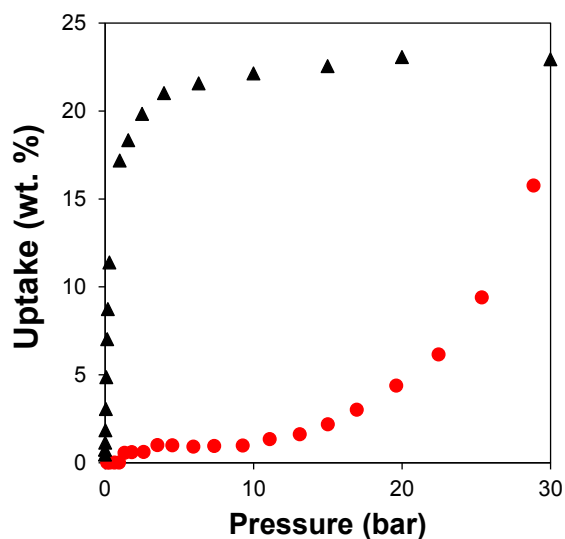


Figure S6. CO₂ experimental, red circles, and simulated, black triangles, adsorption isotherms on **1** at 273 K. The simulated isotherm is able to provide a good estimation of the CO₂ capacity of the material (*ca.* 23 wt. %). Note the big differences at lower pressure where the simulated data overpredict the experimental amount adsorbed.

S5. High-Pressure X-Ray Diffraction

High pressure single crystal study was undertaken using a custom made Diamond Anvil Cell equipped with 0.5 mm culets and a ~40° opening. A small crystal of the sample was loaded in the pre-pressed and drilled steel gasket along with a methanol-ethanol mixture (4:1) and a small ruby sphere for pressure calibration. Data were collected using a single phi scan in the Extreme conditions beamline at Diamond Light Source, using a focused beam of 40 keV as defined by a 20 µm pinhole. Short acquisitions were performed to avoid large radiation damage, anyway visible at the end of the experiment in the form of a brown spot in the center of the crystal. Data were collected using an Agilent Atlas CCD calibrated with a NIST ruby sphere and integrated using the Crysallis package and its high pressure dedicated abilities¹¹. Diamond overlapping peaks were masked out of the integration. Despite attempts no lower or higher symmetry were identified for the given datasets up to 4.5 GPa. The known structure was used for refinement with SHELXL97.ⁱ Due to the small amount of data and their low intrinsic quality aromatic rings were constrained using the AFIX66 routine and other C-C and C-O distances restrained to 1.54 and 1.25 Å respectively. The squeeze routine was applied to correct the intensities from the disorder solvent.

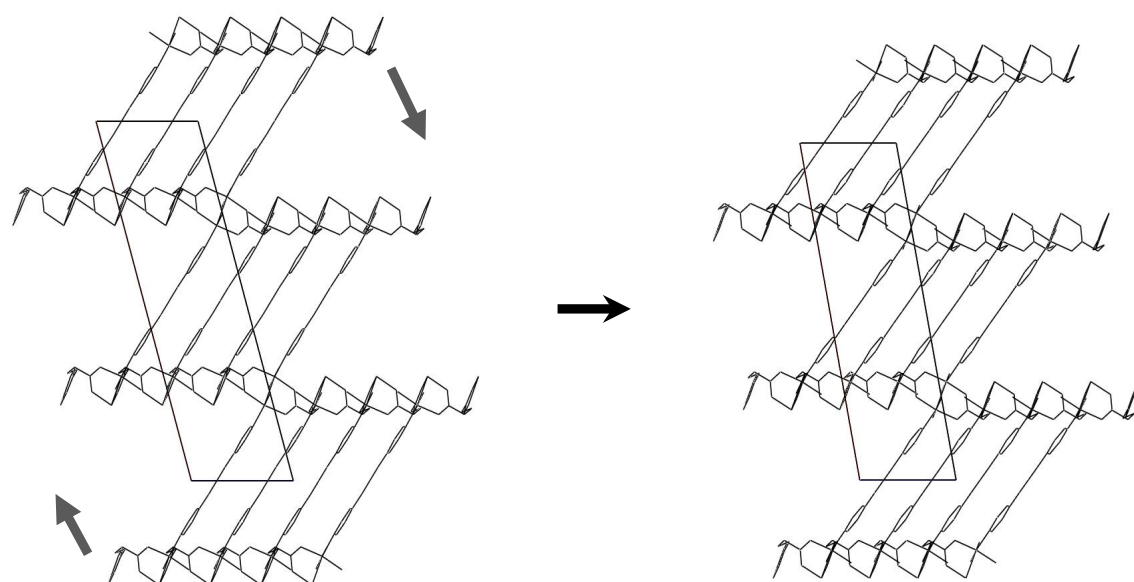


Figure 7. The ambient pressure structure of **1** (*left*) with arrows indicating the deformation modes. On the right, the resulting structure at 4.5 GPa.

S7. References

- 1.- G. M. Sheldrick, *SHELX97*, University of Göttingen, Göttingen, Germany, 1997.
- 2.- A. L. Spek, *PLATON-94 (V-101094), A multipurpose Crystallographic Tool*, University of Utrecht, The Netherlands, 1994.
- 3.- (a) Dubbeldam, D.; Calero, S.; Ellis, D. E.; Snurr, R. Q. RASPA 1.0; Northwestern University: Evanston, IL, 2008;
(b) D. Frenkel and B. Smit, *Understanding Molecular Simulations: From Algorithms to Applications*, 2nd ed., Academic Press, San Diego, 2002.
- 4.- A. K. Rappé, C. J. Casewit, K. S. Colwell, W. A. G. III and W. M. Skiff, *J. Am. Chem. Soc.*, 1992, **114**, 10024-10035
- 5.- M. G. Martin and J. I. Siepmann, *J. Phys. Chem. B*, 1998, **102**, 2569
- 6.- C.E. Wilmer, K.C. Kim and R.Q. Snurr. *J. Phys. Chem. Lett.*, 2012, **3**, pp 2506–2511.
- 7.- Reid, R. C.; Prausnitz, J. M.; Poling, B. E. *The Properties of Gases and Liquids*, 4th ed.; McGraw-Hill: New York, 1987.
- 8.- (a) A. Leach, *Molecular modelling : principles and applications*, Pearson Prentice Hall, 2001.; (b) A. L. Myers and P. A. Monson, *Langmuir*, 2002, **18**, 10261.
- 9.- L. D. Gelb and K. E. Gubbins, *Langmuir*, 1998, **15**, 305-308.
- 10.- I.H. Hwang, J.M. Bae, W.-S. Kim, Y.D. Jo, C. Kim, Y. Kim, S.-J. Kim and S. Huh, *Dalton Trans.*, 2012, **41**, 12759.
- 11.- Oxford Diffraction (2006). Oxford Diffraction Ltd., Abingdon, England.